Reliability Analysis in the Presence of Aleatory Uncertainty

L. G. Crespo, S. P. Kenny & D. P. Giesy
Dynamic Systems and Control Branch,
MS 308, NASA Langley Research Center, Hampton, Virginia, 23681, USA.

ABSTRACT: This paper proposes a method for modeling a system's response using data. In contrast to approaches that identify a limit state function, we focus on the case in which not all uncertain parameters affecting the response are observable and the measured response is corrupted by noise. To this end, the system response is not characterized by a limit state function but instead by a Random Predictor Model (RPM) having a non-parametric structure. Consequently, the resulting failure probability is not a scalar but a random variable. This variable accounts for the aleatory contributions of the model-form uncertainty and the measurement noise into the response. Furthermore, we propose a framework that enables trading off the predicted range of failure probabilities resulting from such an analysis with a measure of risk. In this context, risk is the percentage of all predicted outcomes the analyst is willing to ignore. The reliability analysis of an aeroelastic structure subject to flutter is used to illustrate the ideas proposed.

1 INTRODUCTION

Metamodeling (Simpson, Peplinski, Koch, & Allen 2001) refers to the process of creating a mathematical representation of a phenomenon based on input-output data. This paper uses a metamodeling technique for constructing computational models describing the distribution of a continuous output variable. These models are called *Random Predictor Models* (RPMs) because the predicted output corresponding to any given input is a random variable. One common example of an RPM is a Gaussian Process (GP) model (Rasmussen & Williams 2006, L. Munoz-Gonzales 2016). In contrast to GP models, which only lead unimodal and symmetric responses, we focus on RPMs having a bounded support set and prescribed values for the mean, and the second-, third-, and fourth-order central moment functions. The manipulation of these functions enables the generation of predictors that accurately describe possibly skewed and multimodal responses typical of many physical phenomena.

This paper extends the developments on RPMs made by the authors (Crespo, Giesy, & Kenny 2017a) to account for sampling error in the moment estimates. As an application, we use RPMs for the reliability and risk analysis of a flexible structure. To make the paper self-contained, essential concepts are presented. Supplemental information is available at (Crespo, Giesy, & Kenny 2017b) and (Crespo, Giesy, & Kenny 2017a).

2 PRELIMINARIES

Consider the continuous random variable z with support set[1] $\Delta_z = [z_L, z_U]$, Probability Density Function (PDF) $f_z : \Delta_z \subset \mathbb{R} \to \mathbb{R}^+$, and Cumulative Distribution Function (CDF) $F_z : \Delta_z \to [0, 1]$. Denote by m_r the r-th central moment of z, which is defined as

$$m_r = \int_{\Delta_z} (z - \mu)^r f_z(z) dz, \; r = 0, 1, 2, \ldots \qquad (1)$$

where μ is the expected value of z. Note that $m_0 = 1$, $m_1 = 0$, m_2 is the variance, m_3 is the third-order central moment, and m_4 is the fourth-order central moment. Where reference is made to the r-th moment of a random variable, we assume that the corresponding integral in (1) converges for that distribution.

The random variables of interest will be constrained to have a bounded support set and given values for μ, m_2, m_3, and m_4. The bounded support constraint is $\Delta_z \subseteq \Omega_z$, where $\Omega_z = [\underline{z}, \overline{z}]$, with $\overline{z} \geq \underline{z}$ given, whereas the moment constraints are given by (1). The parameters of these constraints will be grouped into the variable $\theta_z \in \mathbb{R}^6$ given by

$$\theta_z = [\underline{z}, \overline{z}, \mu, m_2, m_3, m_4] \, . \qquad (2)$$

Any random variable z having a support set contained by $[\underline{z}, \overline{z}]$ with moments μ, m_2, m_3, and m_4 must sat-

[1] The support set Δ_z of z with CDF F_z is the minimal closed interval containing $\{z : 0 < F_z(z) < 1\}$.

isfy the feasibility conditions $g(\theta_z) \leq 0$ given in (Crespo, Giesy, & Kenny 2017b). The realizations of θ satisfying these conditions constitute the θ-feasible domain, Θ, defined as

$$\Theta = \{\theta : g(\theta) \leq 0\}. \tag{3}$$

A member of Θ will be called θ-feasible. Determining membership in Θ is a distribution-free assessment applicable to possibly infinitely many random variables satisfying the desired constraints.

A particular class of random variables that can realize most of Θ is proposed in (Crespo, Giesy, & Kenny 2017b). This class is called *staircase* because the PDF of its members is piecewise constant over bins of equal width. Staircase variables, are calculated by solving the convex optimization program

$$\min_{\ell \geq 0} \{J(\theta, n_b) : A(\theta, n_b)\ell = b(\theta), \theta \in \Theta\}, \tag{4}$$

where J is the cost function used for optimization, n_b is the number of bins partitioning Ω_z, ℓ are the PDF values at the bin centers, and $A\ell = b$ are moment matching constraints. Staircase variables enable modeling complex phenomena efficiently. Staircase variables will be denoted as

$$z \sim S_z(\theta_z, n_b, J). \tag{5}$$

When the cost is chosen to be the entropy, E, we obtain a maximal entropy staircase variable (Crespo, Giesy, & Kenny 2017b). The points $\theta \in \Theta$ for which a staircase variable with n_b bins exists constitutes the staircase feasible domain, $\mathcal{S}(n_b)$. As expected, $\mathcal{S}(n_b) \subset \Theta$. A detailed introduction to staircase variables is available at (Crespo, Giesy, & Kenny 2017b).

2.1 *Effects of Sampling Error*

This section evaluates the error caused by estimating the hyper-parameter θ_z in (2) from the measurements $z^{(1)}, \ldots, z^{(N)}$. A natural estimate of the bound is $\Omega_z = [\min_i\{z^{(i)}\}, \max_i\{z^{(i)}\}]$, whereas the moment estimates can be chosen to be the sampling[2] moments $\dot{\mu}$, $\dot{m}_2$, $\dot{m}_3$ and $\dot{m}_4$.

Lets first focus on the error incurred by using Ω_z. Finite values of N make Ω_z an inner approximation to Δ. Scenario optimization (Campi & Garatti 2008) enables bounding the probability of the tails of the PDF of z extending beyond the bound:

$$\mathbb{P}[z \notin \Omega_z] = \kappa q^\top \ell \leq \hat{\epsilon}, \tag{6}$$

where κ is the width of a staircase bin, $\ell \in \mathbb{R}^{n_b}$ is the staircase likelihood at the bins, the i-th component of $q \in \mathbb{R}^{n_b}$ is equal to one when $c_i \notin \Omega_z$ and it is equal to zero otherwise,

$$\hat{\epsilon} = 1 - e^{\log(\beta)/(N-1)}, \tag{7}$$

and β is the confidence parameter. Equation (7) is a formally verifiable, distribution-free and non-asymptotic result applicable to any stationary Data Generating Mechanism (DGM). Scenario optimization theory states that Equation (7) holds with probability greater than $1 - \beta$, where β can be made very small such that it losses any practical significance. This probability is key for obtaining results that are guaranteed independently of the DGM.

We now focus on the error in the sample moments. This error, fully prescribed by the corresponding sampling distributions, can be quantified by using bootstrapping techniques. Alternatively, an asymptotic approximation to the sampling distribution, grounded in the central limit theorem, can be used instead. Such a distribution is given by the normal variables

$$\begin{aligned}
\mu &\sim \mathcal{N}_\mu\left(\dot{\mu}, \sqrt{\frac{\dot{m}_2}{N}}\right), \\
m_2 &\sim \mathcal{N}_{m_2}\left(\dot{m}_2, \sqrt{\frac{\dot{m}_4 - \dot{m}_2^2}{N}}\right), \\
m_3 &\sim \mathcal{N}_{m_3}\left(\dot{m}_3, \sqrt{\frac{\dot{m}_6 - \dot{m}_3^2 - 6\dot{m}_4\dot{m}_2 + 9\dot{m}_2^3}{N}}\right), \\
m_4 &\sim \mathcal{N}_{m_4}\left(\dot{m}_4, \sqrt{\frac{\dot{m}_8 - \dot{m}_4^2 - 8\dot{m}_5\dot{m}_3 + 16\dot{m}_2\dot{m}_3^2}{N}}\right),
\end{aligned} \tag{8}$$

conditional on $\theta \in \Theta$, where $\dot{m}_k$, for $k = 5, 6, 7, 8$ are the sample fifth, sixth, seventh and eighth central-order moments. These expressions correspond to an arbitrarily distributed variable z for a sufficiently large value of N (Kendall & Stuart 1969). For small values of N, bootstrapping techniques often yield a more accurate approximation.

To account for sampling error in the calculation of a staircase variable, the moment matching constraints are replaced by the polynomial inequality constraints

$$\underline{\mu} \leq \mu(\ell) \leq \overline{\mu}, \tag{9}$$

$$\underline{m}_2 \leq m_2(\ell) \leq \overline{m}_2, \tag{10}$$

$$\underline{m}_3 \leq m_3(\ell) \leq \overline{m}_3, \tag{11}$$

$$\underline{m}_4 \leq m_4(\ell) \leq \overline{m}_4, \tag{12}$$

where $\mu(\ell) = r_2\ell$, $m_2(\ell) = r_3\ell - \mu^2$, $m_3(\ell) = r_4\ell - \mu^3 - 3\mu m_2$ and $m_4(\ell) = r_5\ell - 4\mu m_3 - 6\mu^2 m_2 - \mu^4$ are the moments realized by the staircase variable,

[2] Sampling estimates will be denoted with a dot-superscript.

r_i is the i-th row vector of A in (4), and the moment bounds are the $1-\alpha$ confidence intervals corresponding to the sampling distributions, e.g., $\dot{\mu} - 1.96\sqrt{\dot{m}_2/N} \leq \mu(\ell) \leq \dot{\mu} + 1.96\sqrt{\dot{m}_2/N}$ for a 95% confidence interval. Note that the box of moments defined by (9-12) might not be fully contained in Θ.

Sampling error can be accounted for by solving for a maximal entropy staircase variable constrained by Equations (6), and (9-12). The resulting staircase variable will not account for the manner in which the sampling distribution allocates probability within the box of moments. This consideration can be taken into account by using a likelihood-dependent cost, such as

$$J(\ell) = -E(\ell) - \log\{L(\ell)\}, \tag{13}$$

where $L = \mathcal{N}_{\mu(\ell)}\mathcal{N}_{m_2(\ell)}\mathcal{N}_{m_3(\ell)}\mathcal{N}_{m_4(\ell)}$ is the likelihood function corresponding to the sampling distribution.

In summary, staircase variables provide (i) the ability to represent a wide range of density shapes, (ii) the ability to represent most of the feasible space Θ, (iii) the ability to account for the effects of having a limited number of observations, and (iv) the low-computational cost required to efficiently perform various uncertainty quantification tasks.

3 PREDICTOR MODELS

3.1 *Problem Statement*

A DGM is postulated to act on a vector of input variables, $x \in \mathbb{R}^{n_x}$, to produce an output, $y \in \mathbb{R}^{n_y}$. In this article the focus will be on the single-output ($n_y = 1$) multi-input ($n_x \geq 1$) case. The dependency of the output on the input is arbitrary. This covers the case in which y is a function of x with all components of x available (so there is only one output value for each available input), the case in which y is a function of x but not all components of x are available (so there might be infinitely many outputs for each measured input, and the case in which y is an arbitrary random process of x. Assume that N Independent and Identically Distributed (IID) input-output pairs are obtained from a stationary DGM, and denote by $\mathbb{D} = \left\{x^{(i)}, y^{(i)}\right\}$, for $i = 1, \ldots N$ the corresponding data sequence. The main objective of a predictor model is to generate a computational representation of a DGM based on the data in $\mathbb{D}$. Two types of predictors will be used hereafter. An Interval Predictor Model (IPM) (Campi, Calafiore, & Garatti 2009, Crespo, Kenny, & Giesy 2016) yields a bounded interval of output values at any value of the input. The desired IPM is a narrow interval wherein unobserved data will fall with high probability. Conversely, a Random Predictor Model (RPM) yields a random variable at any value of the input. The desired RPM accurately describes the probability distribution governing the DGM. In the context of this article, this description is given by the range and the first four moments of the output.

3.2 *Interval Predictor Models*

This section presents a means to calculate the support set of an RPM. This will be carried out by finding a baseline IPM using the same data sequence $\mathbb{D}$ that will be used to construct the RPM.

An IPM assigns to each instance vector $x \in X \subseteq \mathbb{R}^{n_x}$ a corresponding outcome interval in $Y \subseteq \mathbb{R}$. That is, an IPM is a set-valued map, $I_y : x \to I_y(x) \subseteq Y$, where $I_y(x)$ is the prediction interval. Depending on context, the term IPM will refer to either the function I_y or its graph $\{(x, y) : x \in X, y \in I_y(x)\}$ in $X \times Y$. A nonparametric IPM is given by

$$I_y(x) = \left\{ \left[\underline{y}(x),\ \overline{y}(x)\right],\ \overline{y}(x) \geq \underline{y}(x) \right\}. \tag{14}$$

where the functions $\underline{y}(x)$ and $\overline{y}(x)$ are the lower and upper boundaries of the IPM respectively. A parametric IPM is obtained by associating to each $x \in X$ the set of outputs y that result from evaluating the function $y = M(x, p)$ at all values of p in the set P, so

$$I_y(x, P) = \{y = M(x, p),\ p \in P\}. \tag{15}$$

Attention will be limited to the case in which the output depends linearly on p and arbitrarily on x, so $y = p^\top \varphi(x)$, where $\varphi(x) \in \mathbb{R}^{n_p}$ is an arbitrary basis. Several IPM types can be calculated within this framework. In this paper we use the technique used in (Crespo, Giesy, & Kenny 2017a).

Example 1: Next we use an analytically described DGM of which we have full knowledge. Figure 1 shows the corresponding one percentiles. Note that the support set, moments and modality of the DGM are strongly nonlinear functions of the input. The high concentration of percentile lines at the edge of the support indicates a bimodal structure. $N = 1000$ IID observations were drawn from the DGM to form the data sequence $\mathbb{D}$. This data, shown in Figure 1, was then used to construct an IPM with $n_p = 20$ terms and a Gaussian basis structure. That is, $\varphi_i(x) = e^{-(x-u_i)^2/v_i}$, where $u_i \in \mathbb{R}$ is a center and $v_i \in \mathbb{R}$ is a length-scale parameter, for $i = 1, \ldots n_p$. Centers are uniformly distributed over $X = [-\pi, \pi]$, whereas the length scale parameters are made all equal to $\pi/5$. Figure 1 also shows the resulting IPM. Notice that the IPM tightly encloses all the data as intended. An IPM will be used to describe the support of the DGM, whereas RPMs, introduced next, will be used to characterize its distribution.

3.3 *Random Predictor Models*

An RPM is a mapping that assigns to each input vector $x \in X$ a corresponding random variable $R_y(x)$. A non-parametric RPM is the random variable-valued

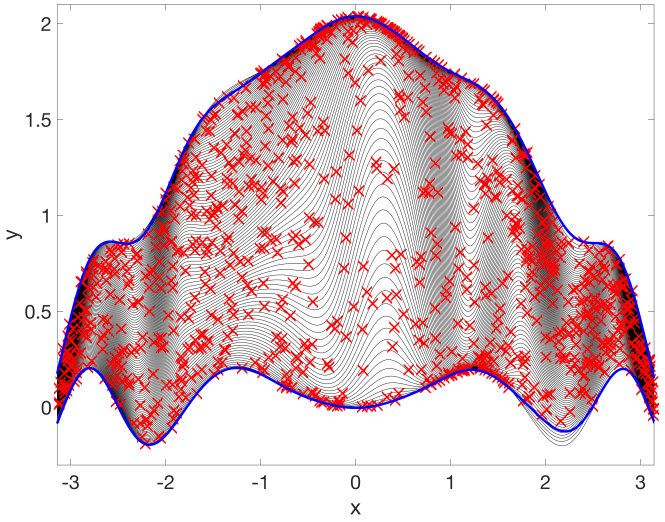

Figure 1. One-percentiles of the DGM (black lines), $N = 1000$ observations (red $\times$), and IPM limits (blue lines).

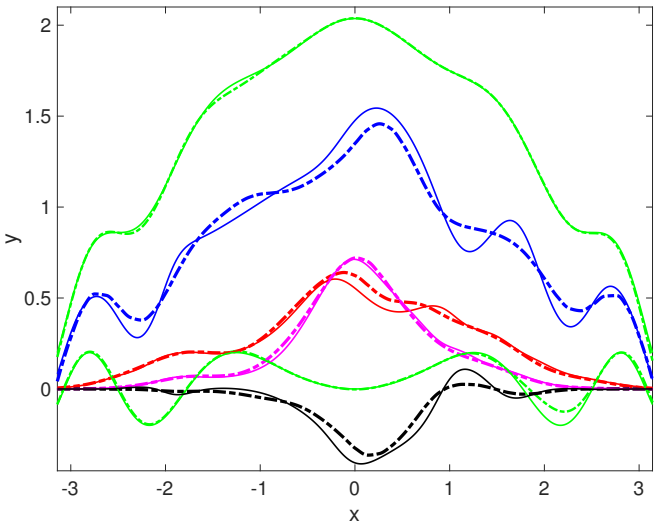

Figure 2. Support set (green), mean (blue), variance (red), third-order- (black), and fourth-order-central moment (magenta) functions corresponding to the DGM (solid) and to the target (dashed-dotted).

map given by

$$R_y(x) = \{f_{y(x)}(y(x)),\ y(x) \in \Delta_y(x)\}, \qquad (16)$$

where $f_{y(x)}$ is the PDF of y at $x \in X$ having the support set $\Delta_y(x) = [\underline{y}(x), \overline{y}(x)] \subseteq Y$. By contrast, a parametric RPM is obtained by associating to each $x \in X$ the set of outputs y corresponding to all values of p described by a random vector with joint PDF $f_p(p)$ supported in Δ_p, so

$$R_y(x, f_p) = \{y = M(x,p),\ p \sim f_p(p),\ p \in \Delta_p\}. \quad (17)$$

The RPMs used below assume a staircase structure. As such, they require prescribing an input-dependent hyper-parameter $h(x) = [n_b(x), \theta_{y(x)}]$ for all $x \in X$. Hereafter we will assume that $n_b(x)$ is a fixed constant, and focus on the prescription of $\theta_{y(x)}$. Define as

$$\tilde{\theta}_{y(x)} = \left[\underline{\tilde{y}}(x), \overline{\tilde{y}}(x), \tilde{\mu}_{y(x)}, \tilde{m}_{2,y(x)}, \tilde{m}_{3,y(x)}, \tilde{m}_{4,y(x)}\right],$$

a set of target functions prescribed according to the data, and by $\theta_{y(x)}$ the set functions realized by an RPM. An RPM that accurately represent the DGM must make $\theta_{y(x)}$ close to $\tilde{\theta}_{y(x)}$. The strategy for prescribing $\tilde{\theta}_{y(x)}$ according to the data sequence $\mathbb{D}$ presented in (Crespo, Giesy, & Kenny 2017b) will be used here. $\tilde{\theta}_{y(x)}$ is based on a weighted average of values $y^{(i)}$ for $x^{(i)}$ close to x.

A non-parametric RPMs with a staircase structure can be readily calculated from the target functions $\tilde{\theta}_{y(x)}$ by making the prediction at any input value $x \in X$ realize the corresponding target. Once a set of staircase-feasible target functions $\tilde{\theta}_{y(x)}$ is obtained, the RPM $S_{y(x)}(\tilde{\theta}_{y(x)}, n_b, J)$ can be readily evaluated at any value of the input. The resulting RPM will conform to the target regardless of the choice of J.

Example 2: Next we use the data sequence of the DGM in Example 1 to derive an RPM. Figure 2 shows the functions in $\theta_{y(x)}$ corresponding to the DGM (solid lines) along with the target functions $\tilde{\theta}_{y(x)}$ (dashed lines). Note that the target functions approximate the DGM well in spite of only using $N = 1000$ observations. The difference between the two sets of functions is caused by the limited amount of data available and by using neighboring data to calculate $\tilde{\theta}_{y(x)}$. The targets $\tilde{\theta}_{y(x)}$ in Figure 2 were used to build the RPM $S_{y(x)}(\tilde{\theta}_{y(x)}, 500, E)$. This RPM is staircase-feasible throughout X. This was also the case for values of n_b as small as 100. The plot at the top of Figure 3 shows the 1-percentiles of this RPM. This figure was generated by calculating staircase variables over a uniform grid of input values in X, sampling them, smoothing the corresponding empirical CDF using a Gaussian kernel (Silverman 1986), and grouping the points belonging to the same percentile line. The moment functions attained by the RPM are indistinguishable from the targets shown in Figure 2. The comparison between the DGM, shown in Figure 1, and the moment-matching RPM indicates excellent agreement despite only using $N = 1000$ data points. Note that RPM describes well the bimodal structure of the DGM by replicating the regions where probability is highly concentrated, i.e., the regions in the upper and lower limit of the support where many percentile lines coalesce. Furthermore the skewness of the probability mass in the interior of the support set follows the same oscillatory patterns present in the DGM.

Example 3: Next we study the effects of the sampling error on the empirical target $\tilde{\theta}_{y(x)}$, and on the resulting staircase RPM. The observations prescribing the target functions at x are weighted according to their separation from such a point (Crespo, Giesy, & Kenny 2017a). The weight is the greatest when the datum is at x, and it approaches zero as its separation

from x increases. For the functions shown in Figure 2, the number of observations having a non-negligible weight ranges from 110 to 261. To quantify the sparsity of the dataset we define the equivalent number of observations, n_e, as

$$n_e(x) = \sum_{i=1}^{N} w\left(x^{(i)}, x\right). \tag{18}$$

As such, the larger the value of n_e the smaller the uncertainty in the sample estimates. The value of n_e corresponding to the functions in Figure 2 range from 47.15 to 112. This indicates that the dataset is sparse. The effects of the sparsity in the data will be quantified using the developments in Section 2.1. In particular, we will generate a maximal entropy RPM satisfying the constraints (6) and (9-12) for $N = n_e(x)$. In contrast to the RPM at the top of Figure 3, the resulting RPM will not match moments estimated from the data but instead, it will realize moment functions bounded by their sample uncertainty. As such, we will refer to this RPM as a moment-bounded RPM. Figure 4 shows the 95% confidence intervals of the four moment functions. Note that the range of these intervals exhibits oscillations, reaching their largest spread near $x = 0$. These regions contain the moments realized by staircase variables comprising the moment-bounded RPM, which are shown as a solid lines. The first three moments vary in the interior of their confidence intervals whereas the fourth moment stays on the lower limit. All but the fourth moment function take on values that vary within the intervals. The uncertainty in the sample moments increases the expected entropy $\mathbb{E}_x[E]$ of the RPM from -0.3642 to 0.7484.

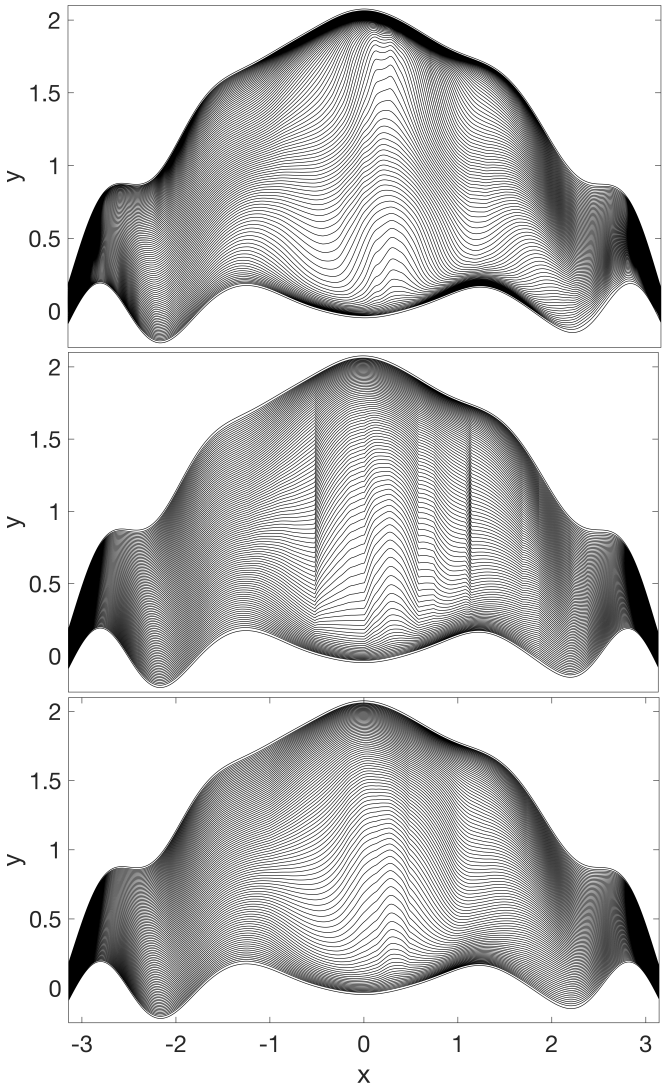

Figure 3. Moment-matching RPM (top), moment-bounded RPM of maximal entropy (middle), and moment-bounded RPM (bottom) based on Equation (13).

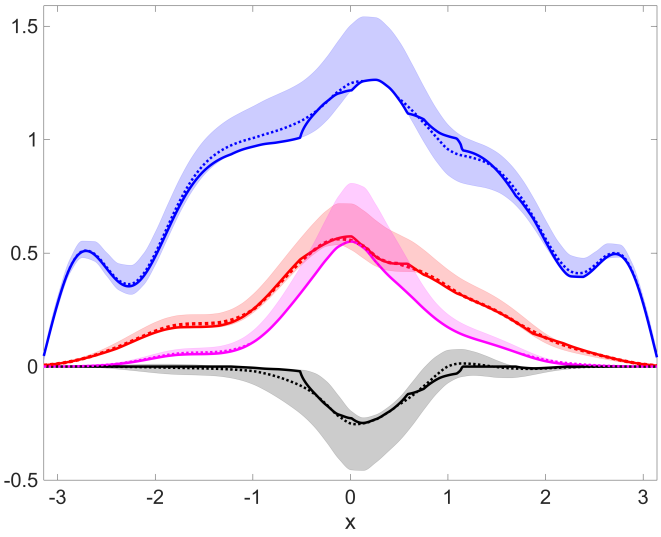

Figure 4. Optimal mean (blue), variance (red), third-order-(black), and fourth-order-central moments (magenta) corresponding to a moment-bounded RPM using maximal entropy (solid lines), Equation (13) (dotted lines), and corresponding sampling error ranges (shaded regions).

Figure 3 shows the moment-matching RPM as well as moment-bounded RPMs of maximal entropy. Note that the most prominent features of the process, such as the peaks at the boundaries of the support set and the patterns of the lines in its interior, have faded in the latter predictor. Furthermore, note that the derivative discontinuities in the moments of Figure 4 yield derivative discontinuities in the percentile lines. Such discontinuities can be eliminated by using a Kernel smoother or by using another cost function. To this end, we calculate a moment-bounded RPM having the cost function in Equation (13). The corresponding moment functions are shown as dotted lines in Figure 4. In contrast to the moments for the maximal entropy formulation, the new moments have continuous derivatives throughout X. The resulting RPM, shown at the bottom of Figure 3, exhibits smooth percentile lines. This is achieved at the expense of a minor entropy reduction to $\mathbb{E}_x[E] = 0.73$. As n_e increases, the width of the confidence intervals reduces making moment-bounded RPMs converge to the moment-matching RPM.

Example 4: Next we consider the reliability analy-

sis (Rackwitz 2001) of an airfoil subject to aeroelastic flutter (Mahler, Touze, Doare, Habib, & Kerschen 2017). During flutter the pitch and plunge dynamics are coupled yielding a self-sustaining limit cycle oscillation that might compromise the structural integrity of an aircraft. The onset of flutter depends on the free stream airflow speed v, as well as inertial, geometrical, and material properties of the wing. These parameters include the plunge and pitch stiffnesses, the aerodynamic lift, the location of the center of mass, and the location of the elastic axis. In this context, a reliability analysis seeks to quantify the probability of flutter instability (i.e., probability of failure) given probabilistic prescriptions for the parameters.

The objectives of this example are two-fold. First, we use RPMs to characterize the system response. Measurement error and model-form uncertainty make the data and the response aleatory, thereby justifying such a modeling choice. A deterministic response model along with a probabilistic description of the parametric uncertainty would enable the calculation of the failure probability. However, when the response is intrinsically aleatory, the failure probability can only be determined to lie within a range of values. We then explore the reduction in the range of failure probabilities resulting from ignoring a (small) percentage of the responses predicted by the RPM.

The stability of the system is evaluated by calculating the damping coefficient, y (i.e., the output in the context of this paper) of the time response to a given flow speed. As in (Canor, Caracoglia, & Denoel 2015), damping is related to the real part of the eigenvalues of a linear dynamic model. Non-negative values of y denote an unstable system, whereas negatives values correspond to a stable system. Hence, the failure domain is defined as

$$\mathcal{F} = \{x : y(x|v) \geq 0\}. \tag{19}$$

The measured output y depends on measurement errors, as well as epistemic and aleatory uncertainties. In this example we will divide the uncertain parameters into two groups. The primary group consists of measurable parameters having a strong influence on the output (e.g., stiffnesses), whereas the secondary group consist of parameters that are either weakly important, unmeasurable, or unknown to the analyst (e.g., measurement error, unsteady aerodynamics, etc.). In this study the primary group of parameters constitute the input x. Note that variations in the secondary parameters make $y(x)$ aleatory. Hence, in contrast to a standard reliability analysis for which a parametric model explicitly prescribes the dependency of the limit state on the uncertain parameters (Sun, Wang, Rui, & Tong 2017), the limit state we are aiming to identify will not be a deterministic function of all the parameters, but instead a random process depending on the primary parameters. This implies that the failure probability will range on an interval whose spread depends upon the manner in which the RPM describing $y(x)$ crosses zero (failure boundary).

For simplicity in the analysis, x will be assumed to be a single non-dimensional parameter describing the ratio of the pitch and plunge stiffnesses. Independent input-output pairs $\mathbb{D} = \{x_i, y_i\}$ for $i = 1, \dots N$, were obtained by simulating the flutter dynamics of $N = 2500$ individual airfoils. The randomness in the output stems from variability of not only x but also of the secondary aerodynamic and structural parameters affecting y. It is expected that such parameters mostly vary within 10% of their nominal value.

Figure 5 shows the input-output data for the free stream airflow speeds $v = 0.75$, $v = 0.79$, $v = 0.83$, $v = 0.87$, $v = 0.91$, $v = 0.95$. Each chosen airfoil was evaluated at these speeds. Note that the number of data points falling into the failure domain $y \geq 0$ increases with v. In all cases, however, the $y = 0$ manifold is crossed by the nominal response near $x = 2.8$. The response of a calibrated deterministic model, to be referred to as a nominal response, is shown as a solid curve. Whereas the nominal system for all but the greatest speed crosses into the instability region at $x = 2.8$, somewhere in $v \in [0.91, 0.95]$ the curve flips to the opposite side of $y = 0$ (see the bottom plots in Figure 5). Reliability analyses using the nominal responses as the limit states will yield an abrupt discontinuity in the failure probability at that speed. This sudden change in the response is caused by a bifurcation. The manner by which the system transitions into instability (e.g, the region in x becoming unstable first) cannot be inferred from studying the nominal system.

The data for all 6 speeds was processed and the resulting moment functions were calculated. Figure 6 shows these functions and their corresponding uncertainty ranges. Note the high sensitivity of the functions to v. For instance, the variance varies considerably throughout x converging to a small value when x is large. Furthermore, the third-order central moment at $x = 2.15$ goes from being practically zero to being large, first positive and then negative. Features like these, driven by the dynamics of the system, can not be accurately described by a GP model. These functions were then used to calculate a maximal entropy RPM with $n_b = 300$ bins. Figure 7 shows the one-percentile curves for the resulting RPMs. The excursion of individual percentiles into the instability region prescribes the severity (i.e., what is the failure probability for a fixed value of x and v) and the manner (i.e., which x region transitions to instability first) by which flutter occurs.

The crossing $y(x|v) = 0$ occurs over a range of x values. Let's formalize this notion by defining the τ-percentile of the RPM as

$$y_\tau(x|v) = F^{-1}_{y(x|v)}(\tau/100), \tag{20}$$

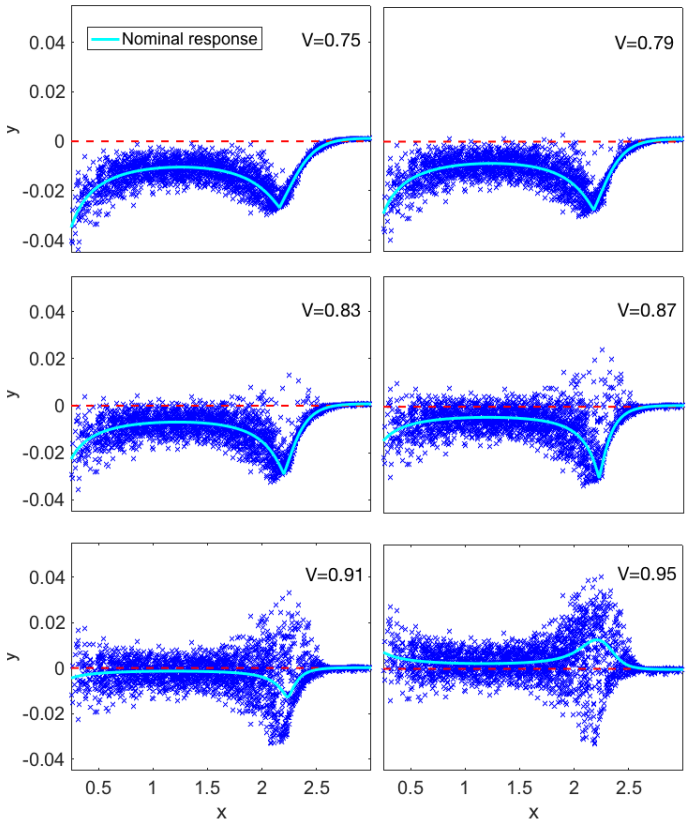

Figure 5. Nominal system response (solid line), and $N = 2500$ observations (blue $\times$) for several airflow speeds.

where $F_{y(x|v)}$ is the distribution of the RPM for speed v, and $\tau \in [0, 100]$ is the percentile of interest. Hence, $y_{100}(x|v)$ is the upper limit of the RPM and $y_0(x|v)$ is the lower limit. The failure domain associated with the τ-percentile at airspeed v is $\mathcal{F}_\tau = \{x : y_\tau(x|v) > 0\}$, whereas the corresponding failure probability is

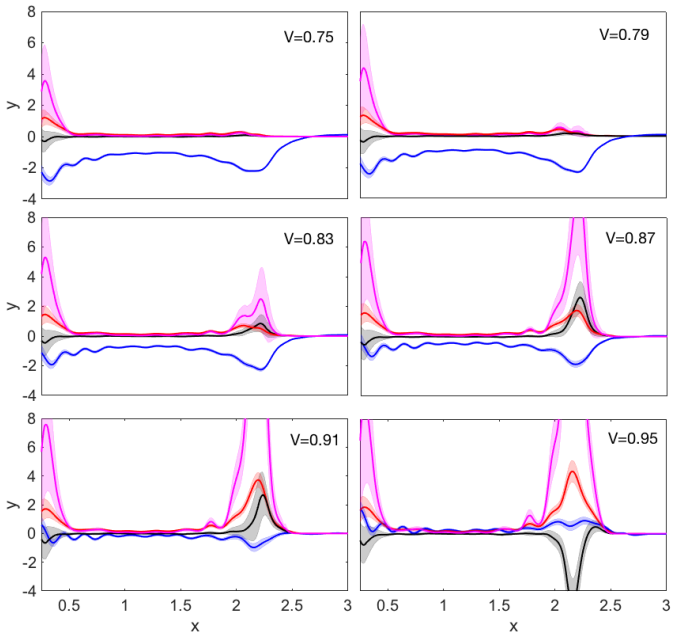

Figure 6. Mean (blue), second- (red), third-(black), and fourth-order (magenta) central moments along with their sampling error ranges (shaded areas).

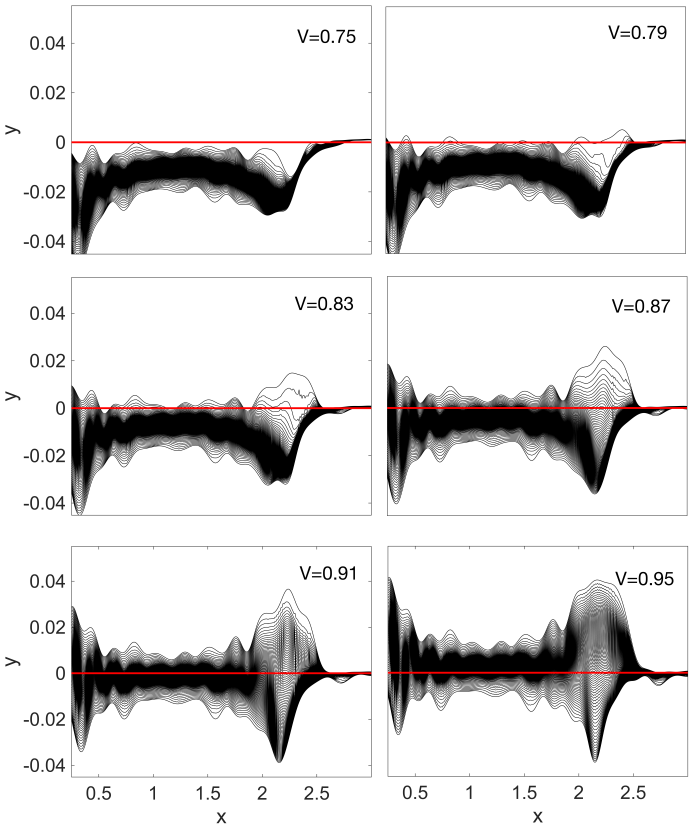

Figure 7: RPMs for several airflow speeds.

$$\mathbb{P}\left[\mathcal{F}_\tau\right] = \int_{\mathcal{F}_\tau} f_x(x)dx, \tag{21}$$

where $f_x(x)$ is the PDF of x. $f_x(x)$ can be prescribed according to the available data or to expert opinion[3]. Modeling the response as an RPM yields the failure probability range

$$r(v) = \left[\, \mathbb{P}[\mathcal{F}_0], \mathbb{P}[\mathcal{F}_{100}] \,\right]. \tag{22}$$

This range can be readily computed for any $f_x(x)$. For instance, if x is a Beta random variable with hyper-parameters 3 and 3 and support $[0, 3]$, we obtain $r(0.75) = [0.0040, 0.0187]$, $r(0.77) = [0.0059, 0.8814]$, $r(0.79) = [0.0024, 0.9948]$. These ranges account for all predicted outputs regardless of their likelihood. The upper limit of some of these ranges is distressingly close to one. However, it is possible that a very small portion of the predicted responses is responsible for most of the spread in the failure probability range. A couple of questions the analyst might contemplate are as follows: If we are willing to ignore some of the worst predicted outputs what will be the corresponding reduction in the failure probability range? How large should be such a reduc-

[3] If the realizations of x in $\mathbb{D}$ were controlled to ensure a good coverage of the response function over the domain of interest X, they should not be used to prescribe a naturally occurring $f_x(x)$, e.g., variations resulting from a manufacturing process.

tion (if any) to justify taking such a risk? By worst-case outputs we mean those leading to the largest decrease in the upper limit of the failure probability range. In this context, the risk, to be denoted as $\zeta \in [0, 100]$, is the percentage of the worst-case predicted responses the analyst is willing to neglect. The analyst might be willing to accept a small risk providing that the corresponding reduction in the failure probability is sufficiently large. This will be the case when the limits of $r(v)$ are prescribed by extreme, low-probability events occurring at the long tail of a distribution. For a given ζ, the failure probability range is given by

$$r(v, \zeta) = [\, \mathbb{P}[\mathcal{F}_0], \mathbb{P}[\mathcal{F}_{100-\zeta}] \,]\,. \tag{23}$$

Figure 8 shows $\mathbb{P}[\mathcal{F}_{100-\zeta}]$ as a function of the risk ζ for several airflow speeds. This figure enables making informed risk-based decisions regarding the reliability assessment of the system. For instance, the range of failure probabilities corresponding to a zero risk for $v = 0.77$ is $r(0.77, 0) = [0.0059, 0.8814]$. These two values correspond to the points on the $v = 0.77$ curve for which the risk is 100 (smallest failure probability) and zero (largest failure probability). This level of risk implies that all predicted outcomes are accounted for. If the analyst is willing to ignore the worst 2 percent of the outputs, Figure 8 leads to $r(0.77, 2) = [0.0059, 0.0193]$. These two values correspond to the points on the $v = 0.77$ curve for which the risk is 100 (smallest failure probability) and 2 (largest failure probability). Therefore, a risk of 2 percent decreases the largest failure probability by 0.8621. This illustrates that a small percentage of the predicted responses is responsible for most of the spread in the range of failure probabilities, and that a risk averse approach might yield an overly conservative prediction. Whereas the zero-risk interval contains *all* predicted responses, the small-risk interval contains *most* of the responses more tightly. This type of information enables the analyst to avoid making overly conservative assessments driven by extreme low-probability events rarely seen in practice.

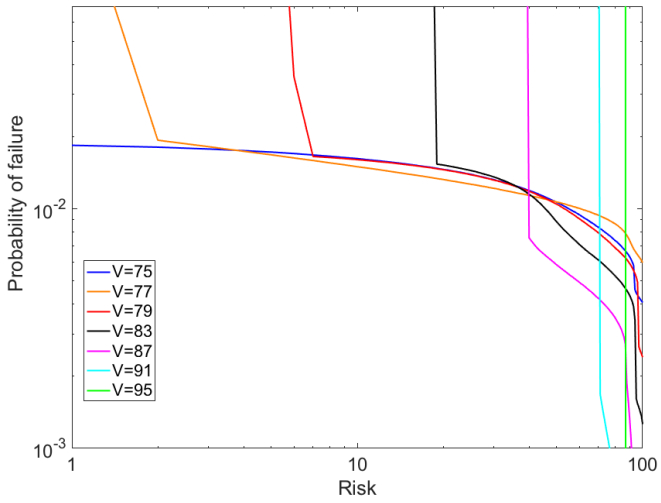

Figure 8: Failure probability vs. risk for several airflow speeds.

4 CONCLUSIONS

This paper illustrates the use of staircase RPMs by applying them to the reliability analysis of an aeroelastic structure. The ability of the staircase variables to describe skewed and multimodal responses over an input-dependent interval makes them well suited for structural dynamics and controls applications. We consider the case in which the predictor is designed to match sample moments exactly (a setting applicable to large datasets), as well as the case in which the predictor accounts for the uncertainty in those estimates (a setting applicable to sparse datasets). The versatility and low computational cost of the proposed framework makes it appropiate for a wide range of applications in science and engineering.

REFERENCES

Campi, M., G. Calafiore, & S. Garatti 2009. Interval predictor models: Identification and reliability. *Automatica 45*(2), 382–392.

Campi, M. C. & S. Garatti 2008. The exact feasibility of randomized solutions of uncertain convex programs. *SIAM Journal on Optimization 19*(3), 1211–1230.

Canor, T., L. Caracoglia, & V. Denoel 2015. Application of random eigenvalue analysis to assess bridge flutter probability. *Journal of wind engineering and industrial aerodynamics 140*, 79–86.

Crespo, L. G., D. P. Giesy, & S. P. Kenny 2017a, June. Nonparametric random predictor models with a staircase structure. In *ESREL 2017, Portoroz, Slovenia*.

Crespo, L. G., D. P. Giesy, & S. P. Kenny 2017b, June. On the calculation and shaping of staircase random variables. In *ESREL 2017, Portoroz, Slovenia*.

Crespo, L. G., S. P. Kenny, & D. P. Giesy 2016. Interval predictor models with a linear parameter dependency. *ASME Journal of verification, validation and uncertainty quantification 1*(2), 1–10.

Kendall, M. & A. Stuart 1969. *The advanced theory of statistics*. London, 3rd edition: Charles, Griffin and Co.

L. Munoz-Gonzales, M. Lazaro-Gredilla, A. F.-V. 2016. Gaussian processes for nonstationary regression. *IEEE transactions on pattern analysis and machine intelligence 38*(3), 618–623.

Mahler, A., C. Touze, O. Doare, G. Habib, & G. Kerschen 2017. Flutter control of a two degrees of freedom airfoil using a nonlinear tuned vibration absorber. *Journal of Computational nonlinear dynamics 12*(5).

Rackwitz, R. 2001. Reliability analysis, a review and some perspectives. *Structural Safety 23*, 365–395.

Rasmussen, C. E. & C. K. Williams 2006. *Gaussian Processes for Machine Learning*. MIT Press.

Silverman, B. W. 1986. *Density Estimation for statistics and data analysis*. 11 New Fetter Lane, London, England: Chapman and Hall.

Simpson, T., J. Peplinski, P. Koch, & J. Allen 2001. Metamodels for computer-based engineering design: survey and recommendations. *Engineering with Computers 17*(1), 129–150.

Sun, Z., J. Wang, L. Rui, & C. Tong 2017. LIF: a new kriging based learning function and its application to structural reliability analysis. *Reliability engineering and system safety 157*, 152–165.